Northumbria Research Link

Citation: Vo, Thuc, Lee, Jaehong and Ahn, Namshik (2009) On sixfold coupled vibrations of thin-walled composite box beams. Composite Structures, 89 (4). 524 - 535. ISSN 0263-8223

Published by: Elsevier

URL: http://dx.doi.org/10.1016/j.compstruct.2008.11.004 <http://dx.doi.org/10.1016/j.compstruct.2008.11.004>

This version was downloaded from Northumbria Research Link: http://nrl.northumbria.ac.uk/13367/

Northumbria University has developed Northumbria Research Link (NRL) to enable users to access the University's research output. Copyright © and moral rights for items on NRL are retained by the individual author(s) and/or other copyright owners. Single copies of full items can be reproduced, displayed or performed, and given to third parties in any format or medium for personal research or study, educational, or not-for-profit purposes without prior permission or charge, provided the authors, title and full bibliographic details are given, as well as a hyperlink and/or URL to the original metadata page. The content must not be changed in any way. Full items must not be sold commercially in any format or medium without formal permission of the copyright holder. The full policy is available online: http://nrl.northumbria.ac.uk/policies.html

This document may differ from the final, published version of the research and has been made available online in accordance with publisher policies. To read and/or cite from the published version of the research, please visit the publisher's website (a subscription may be required.)

www.northumbria.ac.uk/nrl

northumbria UNIVERSITY NEWCASTLE

On sixfold coupled vibrations of thin-walled composite box beams

Thuc Phuong Vo[+], Jaehong Lee[*]

Department of Architectural Engineering, Sejong University

Sejong University, 98 Kunja-dong, Kwangjin-ku, Seoul, 143-747, South Korea

Abstract

This paper presents a general analytical model for free vibration of thin-walled composite beams with arbitrary laminate stacking sequences and studies the effects of shear deformation over the natural frequencies. This model is based on the first-order shear-deformable beam theory and accounts for all the structural coupling coming from the material anisotropy. The seven governing differential equations for coupled flexural-torsional-shearing vibration are derived from the Hamilton's principle. The resulting coupling is referred to as sixfold coupled vibration. Numerical results are obtained to investigate the effects of fiber angle, span-to-height ratio, modulus ratio, and boundary conditions on the natural frequencies as well as corresponding mode shapes of thin-walled composite box beams.

Keywords: Thin-walled composite beams; shear deformation; sixfold coupled vibrations.

[+] Graduate student

[*] Professor, corresponding author. Tel.: +82-2-3408-3287; Fax: +82-2-3408-3331.

E-mail address: jhlee@sejong.ac.kr

On sixfold coupled vibrations of thin-walled composite box beams

Thuc Phuong Vo,* Jaehong Lee,† and Namshik Ahn‡

Department of Architectural Engineering, Sejong University
98 Kunja Dong, Kwangjin Ku, Seoul 143-747, Korea.

(Dated: November 4, 2008)

This paper presents a general analytical model for free vibration of thin-walled composite beams with arbitrary laminate stacking sequences and studies the effects of shear deformation over the natural frequencies. This model is based on the first-order shear-deformable beam theory and accounts for all the structural coupling coming from the material anisotropy. The seven governing differential equations for coupled flexural-torsional-shearing vibration are derived from the Hamilton's principle. The resulting coupling is referred to as sixfold coupled vibration. Numerical results are obtained to investigate the effects of fiber angle, span-to-height ratio, modulus ratio, and boundary conditions on the natural frequencies as well as corresponding mode shapes of thin-walled composite box beams.

Keywords: Thin-walled composite beams; shear deformation; sixfold coupled vibrations.

I. INTRODUCTION

Fiber-reinforced composite materials have been used over the past few decades in a variety of structures. Composites have many desirable characteristics, such as high ratio of stiffness and strength to weight, corrosion resistance and magnetic transparency. Thin-walled structural shapes made up of composite materials, which are usually produced by pultrusion.

Thin-walled beams with closed cross-sections have been widely used in many engineering applications. The vibration characteristics of those members are of fundamental importance in the design of thin-walled structures. The theory

*Graduate student

†Professor, corresponding author. Tel.:+82-2-3408-3287; fax:+82-2-3408-3331

; Electronic address: jhlee@sejong.ac.kr

‡Associate Professor

of thin-walled closed section members made of isotropic materials was first developed by Vlasov [1] and Gjelsvik [2]. Some explicit analytical expressions for the frequency equations and mode shapes of a thin-walled beam with closed cross-section are also available in the literature [3-5]. For thin-walled composite beams, due to material anisotropy, the flexural, torsional and corresponding shearing vibrations are fully coupled even for a doubly symmetric cross-section. Many researchers studied the dynamic analysis of thin-walled closed-section composite beams with various degrees of rigor. Bank and Kao [6,7] focused on the dynamic response and investigated the influence of geometric and material design variables on the free vibration of thin-walled composite material Timoshenko beams. Chandra and Chopra [8] developed theoretical models and closed-form solutions for composite box-beams considering only shear deformation due to bending, however they employed a refined form to describe the warping function and presented extensive comparisons with experimental results. Librescu et al. [9-12] developed models, which were employed in a broad field of engineering problems such as statics and dynamics of composite thin-walled beam. In these models, the bending component of shear flexibility was taken into account but the warping torsion component was neglected. Rand [13] developed theoretical analysis for predicting the natural frequencies and mode shapes of rotating thin-walled composite beams. Armanios and Badir [14] derived the equations of motion for free vibration analysis of anisotropic thin-walled closed-section beams by using a variational asymptotic approach and Hamilton's principle. Based on the governing equations provided by Armanios and Badir [14], Dancila and Armanios [15] isolated the influence of coupling on free vibration of closed-section beams exhibiting extension-twist, bending-twist coupling. Mitra et al. [16] developed a new thin-walled composite beam element of arbitrary cross-section with open or closed contour. The formulation incorporated the effect of elastic coupling, restrained warping, transverse shear deformation associated with thin-walled composite structures. The works of Cortinez, Piovan, Machado and coworkers [17-19] deserved special attention because they introduced a new theoretical model for the generalized linear analysis of thin-walled composite beams. This model allowed studying many problems of static's, free vibrations with or without arbitrary initial stresses and linear stability of composite thin-walled beams. Machado et al. [19] also investigated the dynamic stability of thin-walled composite beams under axial external force. The analysis was based on a small strain and moderate rotation theory, which was formulated through the adoption of a second-order displacement field. In their research [17-19], thin-walled composite beams for both open and closed cross-sections and the shear flexibility (bending, non-uniform warping) were incorporated. However, it was strictly valid for symmetric balanced laminates and especially orthotropic laminates. Shadmehri et al. [20] focused on the static and dynamic characteristics of single-cell thin-walled composite beams. This model incorporated a number of nonclassical effects, such as material

anisotropy, transverse shear, warping inhibition, nonuniform torsional model and rotary inertia. Recently, Vo and Lee [21] presented triply coupled flexural-torsional vibration of thin-walled composite box beam.

In the present paper, the analytical model developed by the authors [22] is extended to the dynamic behavior of thin-walled composite box beams. This model is based on the first-order shear-deformable beam theory, and accounts for all the structural coupling coming from the material anisotropy. The seven governing differential equations for coupled flexural-torsional-shearing vibration are derived from the Hamilton's principle. The resulting coupling is referred to as sixfold coupled vibration. Based on the analytical model, a displacement-based one-dimensional finite element model is developed. Numerical results are obtained to investigate the effects of fiber angle, span-to-height ratio, modulus ratio, and boundary conditions on the natural frequencies and corresponding mode shapes of thin-walled composite box beams.

II. KINEMATICS

The theoretical developments presented in this paper require two sets of coordinate systems which are mutually interrelated. The first coordinate system is the orthogonal Cartesian coordinate system (x, y, z), for which the x and y axes lie in the plane of the cross section and the z axis parallel to the longitudinal axis of the beam. The second coordinate system is the local plate coordinate (n, s, z) as shown in Fig.1, wherein the n axis is normal to the middle surface of a plate element, the s axis is tangent to the middle surface and is directed along the contour line of the cross section. The (n, s, z) and (x, y, z) coordinate systems are related through an angle of orientation θ as defined in Fig.1. Point P is called the pole axis, through which the axis parallel to the z axis is called the pole axis.

To derive the analytical model for a thin-walled composite beam, the following assumptions are made:

1. The contour of the thin wall does not deform in its own plane.

2. Transverse shear strains $\gamma_{xz}^{\circ}, \gamma_{yz}^{\circ}$ and warping shear γ_{ω}° are incorporated. It is assumed that they are uniform over the cross-sections.

3. The linear shear strain $\bar{\gamma}_{sz}$ of the middle surface is to have the same distribution in the contour direction as it does in the St. Venant torsion in each element.

According to assumption 1, the midsurface displacement components $\bar{u}, \bar{v}$ at a point A in the contour coordinate system can be expressed in terms of a displacements U, V of the pole P in the x, y directions, respectively, and the

rotation angle Φ about the pole axis,

$$\bar{u}(s,z) = U(z)\sin\theta(s) - V(z)\cos\theta(s) - \Phi(z)q(s) \tag{1a}$$

$$\bar{v}(s,z) = U(z)\cos\theta(s) + V(z)\sin\theta(s) + \Phi(z)r(s) \tag{1b}$$

These equations apply to the whole contour. The out-of-plane shell displacement $\bar{w}$ can now be found from the assumption 2. For each element of middle surface, the midsurface shear strains in the contour can be expressed with respect to the transverse shear and warping shear strains.

$$\bar{\gamma}_{nz}(s,z) = \gamma^{\circ}_{xz}(z)\sin\theta(s) - \gamma^{\circ}_{yz}(z)\cos\theta(s) + \gamma^{\circ}_{\omega}(z)q(s) \tag{2a}$$

$$\bar{\gamma}_{sz}(s,z) = \gamma^{\circ}_{xz}(z)\cos\theta(s) + \gamma^{\circ}_{yz}(z)\sin\theta(s) - \gamma^{\circ}_{\omega}(z)r(s) - \left[\gamma^{\circ}_{\omega}(z) - \Phi'(z)\right]\frac{F(s)}{t(s)} \tag{2b}$$

where $t(s)$ is thickness of contour box section, $F(s)$ is the St. Venant circuit shear flow.

Further, it is assumed that midsurface shear strain in $s-n$ direction is zero ($\bar{\gamma}_{sn} = 0$). From the definition of the shear strain, $\bar{\gamma}_{sz}$ can also be given for each element of middle surface as:

$$\bar{\gamma}_{sz}(s,z) = \frac{\partial \bar{v}}{\partial z} + \frac{\partial \bar{w}}{\partial s} \tag{3}$$

After substituting for $\bar{v}$ from Eq.(1) into Eq.(3) and considering the following geometric relations

$$dx = ds\cos\theta \tag{4a}$$

$$dy = ds\sin\theta \tag{4b}$$

Displacement $\bar{w}$ can be integrated with respect to s from the origin to an arbitrary point on the contour,

$$\bar{w}(s,z) = W(z) + \Psi_y(z)x(s) + \Psi_x(z)y(s) + \Psi_\omega(z)\omega(s) \tag{5}$$

where Ψ_x, Ψ_y and Ψ_ω represent rotations of the cross section with respect to x, y and ω, respectively, given by

$$\Psi_y = \gamma^{\circ}_{xz}(z) - U' \tag{6a}$$

$$\Psi_x = \gamma^{\circ}_{yz}(z) - V' \tag{6b}$$

$$\Psi_\omega = \gamma^{\circ}_{\omega}(z) - \Phi' \tag{6c}$$

When the transverse shear effect is ignored, Eq.(6) degenerates to $\Psi_y = -U'$, $\Psi_x = -V'$ and $\Psi_\omega = -\Phi'$. As a result, the number of unknown variables reduces to four leading to the Euler-Bernoulli beam model. The prime ($'$) is used

to indicate differentiation with respect to z and ω is the so-called sectorial coordinate or warping function given by

$$\omega(s) = \int_{s_\circ}^{s} \Big[r(s) - \frac{F(s)}{t(s)}\Big] ds \tag{7a}$$

$$\oint_i \frac{F(s)}{t(s)} ds = 2A_i \quad i = 1, .., n \tag{7b}$$

where $r(s)$ is height of a triangle with the base ds; A_i is the area circumscribed by the contour of the i circuit. The explicit forms of $\omega(s)$, $F(s)$ for box section are given in Ref.[23].

The displacement components u, v, w representing the deformation of any generic point on the profile section are given with respect to the midsurface displacements $\bar{u}, \bar{v}, \bar{w}$ by assuming the first order variation of inplane displacements v, w through the thickness of the contour as

$$u(s, z, n) = \bar{u}(s, z) \tag{8a}$$

$$v(s, z, n) = \bar{v}(s, z) + n\bar{\psi}_s(s, z) \tag{8b}$$

$$w(s, z, n) = \bar{w}(s, z) + n\bar{\psi}_z(s, z) \tag{8c}$$

where, $\bar{\psi}_s$ and $\bar{\psi}_z$ denote the rotations of a transverse normal about the z and s axis, respectively. These functions can be determined by considering that the midsurface shear strains γ_{nz} is given by definition

$$\bar{\gamma}_{nz}(s, z) = \frac{\partial \bar{w}}{\partial n} + \frac{\partial \bar{u}}{\partial z} \tag{9}$$

By comparing Eq.(2) and (9), the function $\bar{\psi}_z$ can be written as

$$\bar{\psi}_z = \Psi_y \sin\theta - \Psi_x \cos\theta - \Psi_\omega q \tag{10}$$

Similarly, using the assumption that the shear strain γ_{sn} should vanish at midsurface, the function $\bar{\psi}_s$ can be obtained

$$\bar{\psi}_s = -\frac{\partial \bar{u}}{\partial s} \tag{11}$$

The strains associated with the small-displacement theory of elasticity are given by

$$\epsilon_s(s, z, n) = \bar{\epsilon}_s(s, z) + n\bar{\kappa}_s(s, z) \tag{12a}$$

$$\epsilon_z(s, z, n) = \bar{\epsilon}_z(s, z) + n\bar{\kappa}_z(s, z) \tag{12b}$$

$$\gamma_{sz}(s, z, n) = \bar{\gamma}_{sz}(s, z) + n\bar{\kappa}_{sz}(s, z) \tag{12c}$$

$$\gamma_{nz}(s, z, n) = \bar{\gamma}_{nz}(s, z) + n\bar{\kappa}_{nz}(s, z) \tag{12d}$$

where

$$\bar{\epsilon}_s = \frac{\partial \bar{v}}{\partial s}; \quad \bar{\epsilon}_z = \frac{\partial \bar{w}}{\partial z} \tag{13a}$$

$$\bar{\kappa}_s = \frac{\partial \bar{\psi}_s}{\partial s}; \quad \bar{\kappa}_z = \frac{\partial \bar{\psi}_z}{\partial z} \tag{13b}$$

$$\bar{\kappa}_{sz} = \frac{\partial \bar{\psi}_z}{\partial s} + \frac{\partial \bar{\psi}_s}{\partial z}; \quad \bar{\kappa}_{nz} = 0 \tag{13c}$$

All the other strains are identically zero. In Eq.(13), $\bar{\epsilon}_s$ and $\bar{\kappa}_s$ are assumed to be zero, and $\bar{\epsilon}_z$, $\bar{\kappa}_z$ and $\bar{\kappa}_{sz}$ are midsurface axial strain and biaxial curvature of the shell, respectively. The above shell strains can be converted to beam strain components by substituting Eqs.(1), (5) and (8) into Eq.(13) as

$$\bar{\epsilon}_z = \epsilon_z^\circ + x\kappa_y + y\kappa_x + \omega\kappa_\omega \tag{14a}$$

$$\bar{\kappa}_z = \kappa_y \sin\theta - \kappa_x \cos\theta - \kappa_\omega q \tag{14b}$$

$$\bar{\kappa}_{sz} = \kappa_{sz} \tag{14c}$$

where $\epsilon_z^\circ, \kappa_x, \kappa_y, \kappa_\omega$ and κ_{sz} are axial strain, biaxial curvatures in the x and y direction, warping curvature with respect to the shear center, and twisting curvature in the beam, respectively defined as

$$\epsilon_z^\circ = W' \tag{15a}$$

$$\kappa_x = \Psi_x' \tag{15b}$$

$$\kappa_y = \Psi_y' \tag{15c}$$

$$\kappa_\omega = \Psi_\omega' \tag{15d}$$

$$\kappa_{sz} = \Phi' - \Psi_\omega \tag{15e}$$

The resulting strains can be obtained from Eqs.(12) and (14) as

$$\epsilon_z = \epsilon_z^\circ + (x + n\sin\theta)\kappa_y + (y - n\cos\theta)\kappa_x + (\omega - nq)\kappa_\omega \tag{16a}$$

$$\gamma_{sz} = \gamma_{xz}^\circ \cos\theta + \gamma_{yz}^\circ \sin\theta + \gamma_\omega^\circ (r - \frac{F}{2t}) + \kappa_{sz}(n + \frac{F}{2t}) \tag{16b}$$

$$\gamma_{nz} = \gamma_{xz}^\circ \sin\theta - \gamma_{yz}^\circ \cos\theta - \gamma_\omega^\circ q \tag{16c}$$

III. VARIATIONAL FORMULATION

Total potential energy of the system is calculated by

$$\Pi = \frac{1}{2}\int_v (\sigma_z \epsilon_z + \sigma_{sz}\gamma_{sz} + \sigma_{nz}\gamma_{nz}) dv \tag{17}$$

After substituting Eq.(16) into Eq.(17)

$$\begin{aligned}\Pi &= \frac{1}{2}\int_v \Big\{\sigma_z\Big[\epsilon_z^\circ + (x+n\sin\theta)\kappa_y + (y-n\cos\theta)\kappa_x + (\omega-nq)\kappa_\omega\Big] \\ &+ \sigma_{sz}\Big[\gamma_{xz}^\circ\cos\theta + \gamma_{yz}^\circ\sin\theta + \gamma_\omega^\circ(r-\frac{F}{2t}) + \kappa_{sz}(n+\frac{F}{2t})\Big] + \sigma_{nz}\Big[\gamma_{xz}^\circ\sin\theta - \gamma_{yz}^\circ\cos\theta - \gamma_\omega^\circ q\Big]\Big\}dv \end{aligned} \tag{18}$$

The variation of total potential energy, Eq.(18), can be stated as

$$\delta\Pi = \int_0^l (N_z\delta\epsilon_z + M_y\delta\kappa_y + M_x\delta\kappa_x + M_\omega\delta\kappa_\omega + V_x\delta\gamma_{xz}^\circ + V_y\delta\gamma_{yz}^\circ + T\delta\gamma_\omega^\circ + M_t\delta\kappa_{sz})ds \tag{19}$$

where $N_z, M_x, M_y, M_\omega, V_x, V_y, T, M_t$ are axial force, bending moments in the x- and y-directions, warping moment (bimoment), shear force in the x- and y-direction, and torsional moments with respect to the centroid respectively, defined by integrating over the cross-sectional area A as

$$N_z = \int_A \sigma_z dsdn \tag{20a}$$

$$M_y = \int_A \sigma_z(x+n\sin\theta)dsdn \tag{20b}$$

$$M_x = \int_A \sigma_z(y-n\cos\theta)dsdn \tag{20c}$$

$$M_\omega = \int_A \sigma_z(\omega-nq)dsdn \tag{20d}$$

$$V_x = \int_A (\sigma_{sz}\cos\theta + \sigma_{nz}\sin\theta)dsdn \tag{20e}$$

$$V_y = \int_A (\sigma_{sz}\sin\theta - \sigma_{nz}\cos\theta)dsdn \tag{20f}$$

$$T = \int_A \Big[\sigma_{sz}(r-\frac{F}{2t}) - \sigma_{nz}q\Big]dsdn \tag{20g}$$

$$M_t = \int_A \sigma_{sz}(n+\frac{F}{2t})dsdn \tag{20h}$$

The kinetic energy of the system is given by

$$\mathcal{T} = \frac{1}{2}\int_v \rho(\dot{u}^2 + \dot{v}^2 + \dot{w}^2)dv \tag{21}$$

where ρ is a density.

The variation of the kinetic energy is expressed by substituting the assumed displacement field into Eq.(21) as

$$\begin{aligned}
\delta\mathcal{T} &= \int_v \rho\Big\{\delta\dot{W}\Big[\dot{W}+\dot{\Psi}_x(y-n\cos\theta)+\dot{\Psi}_y(x+n\sin\theta)+\dot{\Psi_\omega}(\omega-nq)\Big] \\
&+ \delta\dot{U}\Big[\dot{U}+\dot{\Phi}\Big[n\cos\theta-(y-y_p)\Big]\Big]+\delta\dot{V}\Big[m_0\dot{V}+\dot{\Phi}\Big[n\sin\theta+(x-x_p)\Big]\Big] \\
&+ \delta\dot{\Phi}\dot{\Phi}\Big[\dot{U}\Big[n\cos\theta-(y-y_p)\Big]+\dot{V}\Big[n\sin\theta+(x-x_p)\Big]+\dot{\Phi}(q^2+r^2+2rn+n^2)\Big] \\
&+ \delta\dot{\Psi}_x\dot{\Psi}_x\Big[\dot{W}(y-n\cos\theta)+\dot{\Psi}_x(y-n\cos\theta)^2+\dot{\Psi}_y(x+n\sin\theta)(y-n\cos\theta)+\dot{\Psi}_\omega(y-n\cos\theta)(\omega-nq)\Big] \\
&+ \delta\dot{\Psi_y}\dot{\Psi}_y\Big[\dot{W}(x+n\sin\theta)+\dot{\Psi}_x(x+n\sin\theta)(y-n\cos\theta)+\dot{\Psi}_y(x+n\sin\theta)^2+\dot{\Psi}_\omega(x+n\sin\theta)(\omega-nq)\Big] \\
&+ \delta\dot{\Psi_\omega}\dot{\Psi}_\omega\Big[\dot{W}(\omega-nq)+\dot{\Psi}_x(y-n\cos\theta)(\omega-nq)+\dot{\Psi}_y(x+n\sin\theta)(\omega-nq)+\dot{\Psi}_\omega(\omega-nq)^2\Big]\Big\}dv
\end{aligned} \tag{22}$$

In Eq.(22), the following geometric relations are used (Fig.1)

$$x-x_p = q\cos\theta+r\sin\theta \tag{23a}$$

$$y-y_p = q\sin\theta-r\cos\theta \tag{23b}$$

In order to derive the equations of motion, Hamilton's principle is used

$$\delta\int_{t_1}^{t_2}(\mathcal{T}-\Pi)dt = 0 \tag{24}$$

Substituting Eqs.(19) and (22) into Eq.(24), the following weak statement is obtained

$$\begin{aligned}
0 &= \int_{t_1}^{t_2}\int_0^l\Big\{\delta\dot{W}\Big[m_0\dot{W}-m_c\dot{\Psi}_x+m_s\dot{\Psi}_y+(m_\omega-m_q)\dot{\Psi_\omega}\Big]+\delta\dot{U}\Big[m_0\dot{U}+(m_c+y_pm_0)\dot{\Phi}\Big] \\
&+ \delta\dot{V}\Big[m_0\dot{V}+(m_s-x_pm_0)\dot{\Phi}\Big]+\delta\dot{\Phi}\Big[(m_c+y_pm_0)\dot{U}+(m_s-x_pm_0)\dot{V}+(m_p+m_2+2m_r)\dot{\Phi}\Big] \\
&+ \delta\dot{\Psi}_x\Big[-m_c\dot{W}+(m_{y2}-2m_{yc}+m_{c2})\dot{\Psi}_x+(m_{xycs}-m_{cs})\dot{\Psi}_y+(m_{y\omega}-m_{y\omega qc}+m_{qc})\dot{\Psi}_\omega\Big] \\
&+ \delta\dot{\Psi}_y\Big[m_s\dot{W}+(m_{xycs}-m_{cs})\dot{\Psi}_x+(m_{x2}+2m_{xs}+m_{s2})\dot{\Psi}_y+(m_{x\omega}+m_{x\omega qs}-m_{qs})\dot{\Psi}_\omega\Big] \\
&+ \delta\dot{\Psi}_\omega\Big[(m_\omega-m_q)\dot{W}+(m_{y\omega}-m_{y\omega qc}+m_{qc})\dot{\Psi}_x+(m_{x\omega}+m_{x\omega qs}-m_{qs})\dot{\Psi}_y+(m_{\omega 2}-2m_{q\omega}+m_{q2})\dot{\Psi}_\omega\Big] \\
&- N_z\delta W'-M_y\delta\Psi_y'-M_x\delta\Psi_x'-M_\omega\delta\Psi_\omega'-V_x\delta(U'+\Psi_y)-V_y\delta(V'+\Psi_x)-T\delta(\Phi'-\Psi_\omega) \\
&- M_t\delta(\Phi'-\Psi_\omega)\Big\}dzdt
\end{aligned} \tag{25}$$

In Eq.(25), the inertia coefficients are defined by

$$m_0 = I_0\int_s ds \tag{26a}$$

$$m_c = I_1 \int_s \cos\theta ds \tag{26b}$$

$$m_r = I_1 \int_s r ds \tag{26c}$$

$$m_p = I_0 \int_s (q^2 + r^2) ds \tag{26d}$$

$$m_q = I_1 \int_s q ds \tag{26e}$$

$$m_s = I_1 \int_s \sin\theta ds \tag{26f}$$

$$m_\omega = I_0 \int_s \omega ds \tag{26g}$$

$$m_2 = I_2 \int_s ds \tag{26h}$$

$$m_{c2} = I_2 \int_s \cos^2\theta ds \tag{26i}$$

$$m_{s2} = I_2 \int_s \sin^2\theta ds \tag{26j}$$

$$m_{q2} = I_2 \int_s q^2 ds \tag{26k}$$

$$m_{x2} = I_0 \int_s x^2 ds \tag{26l}$$

$$m_{y2} = I_0 \int_s y^2 ds \tag{26m}$$

$$m_{\omega 2} = I_0 \int_s \omega^2 ds \tag{26n}$$

$$m_{cs} = I_2 \int_s \sin\theta\cos\theta ds \tag{26o}$$

$$m_{qc} = I_2 \int_s q\cos\theta ds \tag{26p}$$

$$m_{qs} = I_2 \int_s q\sin\theta ds \tag{26q}$$

$$m_{xs} = I_1 \int_s x\sin\theta ds \tag{26r}$$

$$m_{yc} = I_1 \int_s y\cos\theta ds \tag{26s}$$

$$m_{q\omega} = I_1 \int_s q\omega ds \tag{26t}$$

$$m_{x\omega} = I_0 \int_s x\omega ds \tag{26u}$$

$$m_{y\omega} = I_0 \int_s y\omega ds \tag{26v}$$

$$m_{\omega c} = I_1 \int_s \omega\cos\theta ds \tag{26w}$$

$$m_{\omega s} = I_1 \int_s \omega\sin\theta ds \tag{26x}$$

$$m_{xycs} = I_1 \int_s (-x\cos\theta + y\sin\theta) ds \tag{26y}$$

$$m_{x\omega qs} = I_1 \int_s (-qx + \omega\sin\theta) ds \tag{26z}$$

$$m_{y\omega qc} = I_1 \int_s (qy + \omega\cos\theta) ds \tag{26aa}$$

where

$$(I_0, I_1, I_2) = \int_n \rho(1, n, n^2) dn \tag{27}$$

The explicit forms of the inertia coefficients for box section are given in the Appendix.

IV. CONSTITUTIVE EQUATIONS

The constitutive equations of a k^{th} orthotropic lamina in the laminate co-ordinate system of box section are given by

$$\begin{Bmatrix} \sigma_z \\ \sigma_{sz} \end{Bmatrix}^k = \begin{bmatrix} \bar{Q}^*_{11} & \bar{Q}^*_{16} \\ \bar{Q}^*_{16} & \bar{Q}^*_{66} \end{bmatrix}^k \begin{Bmatrix} \epsilon_z \\ \gamma_{sz} \end{Bmatrix} \tag{28}$$

where $\bar{Q}^*_{ij}$ are transformed reduced stiffnesses. The transformed reduced stiffnesses can be calculated from the transformed stiffnesses based on the plane stress ($\sigma_s = 0$) and plane strain ($\epsilon_s = 0$) assumption. More detailed explanation can be found in Ref.[24].

The constitutive relation for out-of-plane stress and strain is given by

$$\sigma_{nz} = \bar{Q}_{55} \gamma_{nz} \tag{29}$$

The constitutive equations for bar forces and bar strains are obtained by using Eqs.(16), (20) and (28)

$$\begin{Bmatrix} N_z \\ M_y \\ M_x \\ M_\omega \\ M_t \\ V_x \\ V_y \\ T \end{Bmatrix} = \begin{bmatrix} E_{11} & E_{12} & E_{13} & E_{14} & E_{15} & E_{16} & E_{17} & E_{18} \\ & E_{22} & E_{23} & E_{24} & E_{25} & E_{26} & E_{27} & E_{28} \\ & & E_{33} & E_{34} & E_{35} & E_{36} & E_{37} & E_{38} \\ & & & E_{44} & E_{45} & E_{46} & E_{47} & E_{48} \\ & & & & E_{55} & E_{56} & E_{57} & E_{58} \\ & & & & & E_{66} & E_{67} & E_{68} \\ & & & & & & E_{77} & E_{78} \\ \text{sym.} & & & & & & & E_{88} \end{bmatrix} \begin{Bmatrix} \epsilon^\circ_z \\ \kappa_y \\ \kappa_x \\ \kappa_\omega \\ \kappa_{sz} \\ \gamma^\circ_{xz} \\ \gamma^\circ_{yz} \\ \gamma^\circ_\omega \end{Bmatrix} \tag{30}$$

where E_{ij} are stiffnesses of the thin-walled composite beams. The explicit forms of laminate stiffness E_{ij} for the thin-walled composite box beams are given in Ref.[22].

V. EQUATIONS OF MOTION

The equations of motion of the present study can be obtained by integrating the derivatives of the varied quantities by parts and collecting the coefficients of $\delta W, \delta U, \delta V, \delta\Phi, \delta\Psi_y, \delta\Psi_x$ and $\delta\Psi_\omega$

$$N_z' = m_0\ddot{W} - m_c\ddot{\Psi}_x + m_s\ddot{\Psi}_y + (m_\omega - m_q)\ddot{\Psi}_\omega \tag{31a}$$

$$V_x' = m_0\ddot{U} + (m_c + y_p m_0)\ddot{\Phi} \tag{31b}$$

$$V_y' = m_0\ddot{V} + (m_s - x_p m_0)\ddot{\Phi} \tag{31c}$$

$$M_t' + T' = (m_c - m_y + y_p m_0)\ddot{U} + (m_s - x_p m_0)\ddot{V} + (m_p + m_2 + 2m_r)\ddot{\Phi} \tag{31d}$$

$$M_y' - V_x = m_s\ddot{W} + (m_{xycs} - m_{cs})\ddot{\Psi}_x + (m_{x2} + 2m_{xs} + m_{s2})\ddot{\Psi}_y + (m_{x\omega} + m_{x\omega qs} - m_{qs})\ddot{\Psi}_\omega \tag{31e}$$

$$M_x' - V_y = -m_c\ddot{W} + (m_{y2} - 2m_{yc} + m_{c2})\ddot{\Psi}_x + (m_{xycs} - m_{cs})\ddot{\Psi}_y + (m_{y\omega} - m_{y\omega qc} + m_{qc})\ddot{\Psi}_\omega \tag{31f}$$

$$\begin{aligned} M_\omega' + M_t - T &= (m_\omega - m_q)\ddot{W} + (m_{y\omega} - m_{y\omega qc} + m_{qc})\ddot{\Psi}_x + (m_{x\omega} + m_{x\omega qs} - m_{qs})\ddot{\Psi}_y \\ &+ (m_{\omega 2} - 2m_{q\omega} + m_{q2})\ddot{\Psi}_\omega \end{aligned} \tag{31g}$$

The natural boundary conditions are of the form

$$\delta W : \quad W = \overline{W}_0 \quad \text{or} \quad N_z = \overline{N}_{z_0} \tag{32a}$$

$$\delta U : \quad U = \overline{U}_0 \quad \text{or} \quad V_x = \overline{V}_{x_0} \tag{32b}$$

$$\delta V : \quad V = \overline{V}_0 \quad \text{or} \quad V_y = \overline{V}_{y_0} \tag{32c}$$

$$\delta\Phi : \quad \Phi = \overline{\Phi}_0 \quad \text{or} \quad T + M_t = \overline{T}_0 + \overline{M}_{t_0} \tag{32d}$$

$$\delta\Psi_y : \quad \Psi_y = \overline{\Psi}_{y_0} \quad \text{or} \quad M_y = \overline{M}_{y_0} \tag{32e}$$

$$\delta\Psi_x : \quad \Psi_x = \overline{\Psi}_{x_0} \quad \text{or} \quad M_x = \overline{M}_{x_0} \tag{32f}$$

$$\delta\Psi_\omega : \quad \Psi_\omega = \overline{\Psi}_{\omega_0} \quad \text{or} \quad M_\omega = \overline{M}_{\omega_0} \tag{32g}$$

The 7^{th} denotes the warping restraint boundary condition. When the warping of the cross section is restrained, $\Psi_\omega = 0$ and when the warping is not restrained, $M_\omega = 0$.

Eq.(31) is most general form for axial-flexural-torsional-shearing vibration of the thin-walled composite beams. For general anisotropic materials, the dependent variables W, U, V, Φ, Ψ_x, Ψ_y and Ψ_ω are fully-coupled implying that the beam undergoes a coupled behavior involving extension, bending, twisting, transverse shearing, and warping. The resulting coupling is referred to as sixfold coupled vibrations. If all the coupling effects are neglected and cross section is symmetrical with respect to both x- and the y-axes, Eq.(31) can be simplified to the uncoupled differential

equations as

$$(EA)_{com}W'' = \rho A\ddot{W} \tag{33a}$$

$$(GA_y)_{com}(U'' + \Psi_y') = \rho A\ddot{U} \tag{33b}$$

$$(GA_x)_{com}(V'' + \Psi_x') = \rho A\ddot{V} \tag{33c}$$

$$\Big[(GJ_1)_{com} + (GJ_3)_{com}\Big]\Phi'' - (GJ_2)_{com}\Psi_\omega' = \rho I_p\ddot{\Phi} \tag{33d}$$

$$(EI_y)_{com}\Psi_y'' - (GA_y)_{com}(U' + \Psi_y) = \rho I_y\ddot{\Psi}_y \tag{33e}$$

$$(EI_x)_{com}\Psi_x'' - (GA_x)_{com}(V' + \Psi_x) = \rho I_x\ddot{\Psi}_x \tag{33f}$$

$$(EI_\omega)_{com}\Psi_\omega'' + (GJ_2)_{com}\Phi' - \Big[(GJ_1)_{com} - (GJ_3)_{com}\Big]\Psi_\omega = \rho I_\omega\ddot{\Psi}_\omega \tag{33g}$$

From above equations, $(EA)_{com}$ represents axial rigidity, $(GA_x)_{com}$, $(GA_y)_{com}$, $(GA_\omega)_{com}$ represent shear rigidities with respect to x- and y-axis, $(EI_x)_{com}$ and $(EI_y)_{com}$ represent flexural rigidities with respect to x- and y-axis, $(EI_\omega)_{com}$ represents warping rigidity, and $(GJ_1)_{com}$, $(GJ_2)_{com}$, $(GJ_3)_{com}$, $(GJ)_{com}$ represent torsional rigidities of the thin-walled composite beams, respectively, written as

$$(EA)_{com} = E_{11} \tag{34a}$$

$$(EI_y)_{com} = E_{22} \tag{34b}$$

$$(EI_x)_{com} = E_{33} \tag{34c}$$

$$(EI_\omega)_{com} = E_{44} \tag{34d}$$

$$(GA_y)_{com} = E_{66} \tag{34e}$$

$$(GA_x)_{com} = E_{77} \tag{34f}$$

$$(GA_\omega)_{com} = E_{88} \tag{34g}$$

$$(GJ_1)_{com} = E_{55} + E_{88} \tag{34h}$$

$$(GJ_2)_{com} = E_{55} - E_{88} \tag{34i}$$

$$(GJ_3)_{com} = 2E_{58} \tag{34j}$$

$$(GJ)_{com} = 2E_{55} + 2E_{58} \tag{34k}$$

In Eq.(33), I_p denotes the polar moment of inertia. It is well known that the three distinct vibration modes, flexural vibration in the x- and y-direction and torsional vibration, are identified in this case and the corresponding vibration frequencies are given by the approximate solution or orthotropy solution for a clamped beam boundary conditions [5]

$$\omega_{x_n} = \sqrt{\Big[\frac{\rho A}{(EI_y)_{com}}\frac{L^4}{(n+0.5)^4\pi^4} + \frac{\rho A}{(GA_y)_{com}}\frac{L^2}{n^2\pi^2}\Big]^{-1}} \tag{35a}$$

$$\omega_{y_n} = \sqrt{\Big[\frac{\rho A}{(EI_x)_{com}}\frac{L^4}{(n+0.5)^4\pi^4} + \frac{\rho A}{(GA_x)_{com}}\frac{L^2}{n^2\pi^2}\Big]^{-1}} \tag{35b}$$

$$\omega_{\theta_n} = \sqrt{\Big[\frac{\rho I_p}{(EI_\omega)_{com}}\frac{L^4}{(n+0.5)^4\pi^4} + \frac{\rho I_p}{(GA_\omega)_{com}}\frac{L^2}{n^2\pi^2}\Big]^{-1} + \frac{(GJ)_{com}}{\rho I_p}\frac{n^2\pi^2}{L^2}} \tag{35c}$$

where $\omega_{x_n}, \omega_{y_n}, \omega_{\theta_n}$ are flexural frequencies in the x- and y-direction, and torsional vibration frequency, respectively.

VI. FINITE ELEMENT FORMULATION

The present theory for thin-walled composite beams described in the previous section was implemented via a one-dimensional displacement-based finite element method. The generalized displacements are expressed over each element as a linear combination of the one-dimensional Lagrange interpolation function $\widehat{\phi_j}$ associated with node j and the nodal values

$$W = \sum_{j=1}^{n} w_j\widehat{\phi_j} \tag{36a}$$

$$U = \sum_{j=1}^{n} u_j\widehat{\phi_j} \tag{36b}$$

$$V = \sum_{j=1}^{n} v_j\widehat{\phi_j} \tag{36c}$$

$$\Phi = \sum_{j=1}^{n} \phi_j\widehat{\phi_j} \tag{36d}$$

$$\Psi_y = \sum_{j=1}^{n} \psi_{yj}\widehat{\phi_j} \tag{36e}$$

$$\Psi_x = \sum_{j=1}^{n} \psi_{xj}\widehat{\phi_j} \tag{36f}$$

$$\Psi_\omega = \sum_{j=1}^{n} \psi_{\omega j}\widehat{\phi_j} \tag{36g}$$

Substituting these expressions into the weak statement in Eq.(22), the finite element model of a typical element can be expressed as

$$([K] - \lambda[M])\{\Delta\} = \{0\} \tag{37}$$

where $[K]$ is the element stiffness matrix

$$[K] = \begin{bmatrix} K_{11} & K_{12} & K_{13} & K_{14} & K_{15} & K_{16} & K_{17} \\ & K_{22} & K_{23} & K_{24} & K_{25} & K_{26} & K_{27} \\ & & K_{33} & K_{34} & K_{35} & K_{36} & K_{37} \\ & & & K_{44} & K_{45} & K_{46} & K_{47} \\ & & & & K_{55} & K_{56} & K_{57} \\ & & & & & K_{66} & K_{67} \\ \text{sym.} & & & & & & K_{77} \end{bmatrix} \tag{38}$$

and $[M]$ is the element mass matrix

$$[M] = \begin{bmatrix} M_{11} & M_{12} & M_{13} & M_{14} & M_{15} & M_{16} & M_{17} \\ & M_{22} & M_{23} & M_{24} & M_{25} & M_{26} & M_{27} \\ & & M_{33} & M_{34} & M_{35} & M_{36} & M_{37} \\ & & & M_{44} & M_{45} & M_{46} & M_{47} \\ & & & & M_{55} & M_{56} & M_{57} \\ & & & & & M_{66} & M_{67} \\ \text{sym.} & & & & & & M_{77} \end{bmatrix} \tag{39}$$

More detailed explanation explicit forms of $[K]$ can be found in Ref.[25]. The explicit forms of $[M]$ are given by

$$M_{ij}^{11} = M_{ij}^{22} = M_{ij}^{33} = \int_0^l m_0 \psi_i \psi_j dz \tag{40a}$$

$$M_{ij}^{15} = \int_0^l m_s \psi_i \psi_j dz \tag{40b}$$

$$M_{ij}^{16} = -\int_0^l m_c \psi_i \psi_j dz \tag{40c}$$

$$M_{ij}^{17} = \int_0^l (m_\omega - m_q) \psi_i \psi_j dz \tag{40d}$$

$$M_{ij}^{24} = \int_0^l (m_c + m_0 y_p) \psi_i \psi_j dz \tag{40e}$$

$$M_{ij}^{34} = \int_0^l (m_s - m_0 x_p) \psi_i \psi_j dz \tag{40f}$$

$$M_{ij}^{44} = \int_0^l (m_p + m_2 + 2m_r) \psi_i \psi_j dz \tag{40g}$$

$$M_{ij}^{55} = \int_0^l (m_{x2} + 2m_{xs} + m_{s2}) \psi_i \psi_j dz \tag{40h}$$

$$M_{ij}^{56} = \int_0^l (m_{xycs} - m_{cs}) \psi_i \psi_j dz \tag{40i}$$

$$M_{ij}^{57} = \int_0^l (m_{x\omega} + m_{x\omega qs} - m_{qs})\psi_i\psi_j dz \tag{40j}$$

$$M_{ij}^{66} = \int_0^l (m_{y2} - 2m_{yc} + m_{c2})\psi_i\psi_j dz \tag{40k}$$

$$M_{ij}^{67} = \int_0^l (m_{y\omega} - m_{y\omega qc} + m_{qc})\psi_i\psi_j dz \tag{40l}$$

$$M_{ij}^{77} = \int_0^l (m_{\omega 2} - 2m_{q\omega} + m_{q2})\psi_i\psi_j dz \tag{40m}$$

All other components are zero. In Eq.(37), $\{\Delta\}$ is the eigenvector of nodal displacements corresponding to an eigenvalue

$$\{\Delta\} = \{W\ U\ V\ \Phi\ \Psi_y\ \Psi_x\ \Psi_\omega\}^{\mathrm{T}} \tag{41}$$

VII. NUMERICAL EXAMPLES

For verification purpose, a cantilever composite box beam with material properties and geometric characteristics shown in Table I is considered. Plane stress assumption ($\sigma_s = 0$) is made in the analysis. The natural frequencies obtained from the present analysis are given in Table II, along with the analytical and experimental results of Chandra and Chopra [8] and the finite element results of Librescu and Qin [10]. The first natural frequencies associated with twist-vertical bending coupling, the vertical bending are denoted by 1TV and 1VB, respectively. Results obtained from previous research [21] based on the classical beam theory are also displayed. It is observed that the present results are in good agreement with the solutions in Refs.[8,10] for all cases of lay-ups.

The next example is the same as before except the laminate stacking sequence. An asymmetric composite box beam configuration ($[0/90]_A$) has a ply orientation of $[0_3/90_3]$ and $[90_3/0_3]$ in the top and bottom flanges and similar in the left and right webs. The results are compared with those presented by Mitra et al. [16] in Table III. For the validation of the results in [16], the 3-D finite element results were obtained using ANSYS general purpose program, where eight noded brick element was used to model the structure. The table shows an excellent agreement between the predictions of the present model and the results of the other models mentioned.

In order to investigate the coupling and effects of shear deformation on the natural frequencies and mode shapes, thin-walled composite box beam with geometry and stacking sequences shown in Fig.2 is considered. The following engineering constants are used

$$E_1/E_2 = 25, G_{12}/E_2 = 0.6, G_{12} = G_{13} = G_{23}, \nu_{12} = 0.25 \tag{42}$$

For convenience, the following nondimensional natural frequency is used

$$\bar{\omega} = \frac{\omega l^2}{b_1}\sqrt{\frac{\rho}{E_2}} \tag{43}$$

A clamped composite beam with the left and right webs are considered as angle-ply laminates $[\theta/-\theta]$ and $[-\theta/\theta]$ and similar in the top and bottom flanges (Fig.2a). For this lay-up, all the coupling stiffnesses are zero, but E_{25}, E_{35}, E_{28}, E_{38} do not vanish due to unsymmetric stacking sequence of the flanges and webs. Fig.3 shows the effects of shear deformation on the first three natural frequencies with ratio ($l/b_1 = 20$). The finite element solution with no shear is calculated by previous paper [21]. It is interesting to note that the shear effects are negligbly small even for the lower span-to-height ratio, especially in the interval $\theta \in [30°, 90°]$. As expected, for classical beam model [21], the lowest two natural frequencies ω_1, ω_2 decrease monotonically with the increase of fiber angle. However, for present model, after ω_1, ω_2 reach local maximum values around $\theta = 8°$ and $11°$, respectively, they decrease. These local maximum occur because at low fiber angle large shear effects reduce flexural stiffnesses. As fiber angle increases, these effects become immaterial because of low anisotropic. This trend can be explained that flexural stiffnesses decrease significantly with increasing fiber angle, and thus, the relative shear effects become smaller for the higher fiber angles. The first three natural frequencies by the finite element analysis and the orthotropy solution, which neglects the coupling effects from Eqs.(35a)-(35c) for each mode are given in Table IV. For unidirectional fiber direction, these natural frequencies by the finite element analysis exactly correspond to the first flexural mode in x-direction, the first flexural mode in y-direction and the torsional mode by the orthotropy solution, respectively. As the fiber angle increases, however, this order is changing. It can be explained partly by the mode shapes corresponding to ω_1, ω_2 and ω_3 with fiber angle $\theta = 15°$ in Figs.4-6. In each mode the amplitude along the beam length is nomalized with respect to the maximum amplitude for that mode. All three modes exhibit fourfold coupled vibrations. While mode 1, 3 show the first and the second flexural in x-direction, torsional and corresponding shearing vibration, mode 2 displays the first flexural in y-direction, torsional and corresponding shearing vibration. Due to the small coupling stiffnesses E_{25}, E_{35}, E_{28}, E_{38}, these modes become predominantly the first flexural mode in x-direction, the first flexural mode in y-direction and the second flexural mode in x-direction, respectively, with a little contribution from torsion. Therefore, the results by the finite element analysis and orthotropy solution show slight discrepancy in Table IV. It is indicated that the simple orthotropy solution is sufficiently accurate in this case.

To investigate the coupling and shear effects further, the same configuration with the previous example except the lay-up is considered. Stacking sequence of the bottom flange and the right web are $[\theta_2]$, while the top flange and the left web are [0/45], (Fig.2b). All the coupling stiffnesses, especially, $E_{12}, E_{17}, E_{18}, E_{23}, E_{27}, E_{36}, E_{37}$ and E_{57} become

no more negligibly small. Figs.7 and 8 display the effects of shear deformation on the first three natural frequencies with two different ratios ($l/b_1 = 20$) and ($l/b_1 = 50$). These figures reveal that the solutions excluding shear effects remarkably underestimate the natural frequencies for all the range of fiber angle even for higher span-to-height ratio ($l/b_1 = 50$). This implies that discarding shear deformation leads to an overprediction of the natural frequencies. It is also indicated that the coupling effects become significant because the transverse shear little affects the behavior of this beam ($l/b_1 = 50$). The typical mode shapes corresponding to the lowest three natural frequencies with fiber angle $\theta = 30^\circ$ are illustrated in Figs.9-11. It is from these figures that highlight the influence of shear effects on the free vibration of beam. Relative measures of flexural displacements, torsional and shearing rotation show that all three modes are strong coupling with sixfold coupled vibration (flexural mode in the x-, y-direction, torsional mode and corresponding shearing vibration). These responses are never observed in the classical beam model [21] because the shear effects are not present. This fact explains as the fiber angle changes, the orthotropy solution and the finite element analysis solution show significant discrepancy in Table V. That is, the orthotropy solution is no longer valid for unsymmetrically laminated beams, and sixfold coupled flexural-torsional-shearing vibration should be considered simultaneously even for a doubly symmetric cross-section.

The next example shows the effects of modulus ratio (E_1/E_2) on the natural frequencies $\omega_{x_1}, \omega_{y_1}, \omega_{\theta_1}$ for a simply supported and cantilever composite beam with ratio ($l/b_1 = 10$). The stacking sequence of the webs are $[0/90]_s$ and flanges are unidirectional, (Fig.2c). Since all the coupling stiffnesses vanish, the three distinct vibration mode, flexural vibration in the x- and y-direction and torsional vibration are identified. It can be seen in Fig.12 that with increasing orthotropy ratio (E_1/E_2), omission of shear effects causes an overestimation of ω_{x_1} and ω_{y_1} for simply supported boundary condition. Conversely, torsional natural frequency is almost invariant. It can be explained from Eq.(35c) that the torsional natural frequency is dominated by the torsional rigidity rather than warping rigidity. Moreover, effects of warping is negligibly small for box section. Effect of the warping restraint on the natural frequencies $\omega_{x_1}, \omega_{y_1}, \omega_{\theta_1}$ of a cantilever composite beam with respect to modulus ratio variation is displayed in Fig.13. As ratio (E_1/E_2) increases, this figure reveals that the warping restraint has a stiffening effect. Consequently, the significant discrepancy between warping restraint (WR) and free warping (FW) models occurs only on the the torsional mode, while flexural modes the influence of warping becomes immaterial. It can be explained that torsion is completely decoupled from the flexure and transverse shear in this case.

VIII. CONCLUDING REMARKS

An analytical model based on shear-deformable beam theory is derived to study the free vibration of thin-walled composite box beam. This model is capable of predicting accurate the natural frequencies as well as vibration mode shapes for various configuration including boundary conditions, laminate orientation and span-to-height ratio. To formulate the problem, a one-dimensional displacement-based finite element method is employed. All of the possible vibration modes including the flexural mode in the x- and y-direction, torsional mode, corresponding shearing mode, and fully coupled flexural-torsional-shearing mode are included in the analysis. The resulting coupling is referred to as sixfold coupled vibrations. The present model is found to be appropriate and efficient in analyzing free vibration problem of thin-walled composite beam.

Acknowledgments

The support of the research reported here by Seoul R&BD Program through Grant GR070033 and by Korea Ministry of Construction and Transportation through Grant 2006-C106A1030001-06A050300220 is gratefully acknowledged. The authors also would like to thank the anonymous reviewers for their suggestions in improving the standard of the manuscript.

APPENDIX

The explicit expressions of inertia coefficients for composite box section in Fig.14 are given by

$$m_0 = I_0^1 b_1 + I_0^2 b_2 + I_0^3 b_1 + I_0^4 b_2 \tag{44a}$$

$$m_c = I_1^2 b_2 - I_1^4 b_2 \tag{44b}$$

$$m_r = I_1^1(-x_1 b_1 + x_p b_1) + I_1^2(-y_2 b_2 + y_p b_2) + I_1^3(x_3 b_1 - x_p b_1) + I_1^4(y_4 b_2 - y_p b_2) \tag{44c}$$

$$\begin{aligned} m_p &= I_0^1\Big[\frac{1}{3}b_1^3 + \frac{1}{2}(-2y_4 + 2y_p)b_1^2 + (-y_4 + y_p)^2 b_1 + (-x_1 + x_p)^2 b_1\Big] \\ &+ I_0^2\Big[\frac{1}{3}b_2^3 + \frac{1}{2}(2x_1 - 2x_p)b_2^2 + (x_1 - x_p)^2 b_2 + (-y_2 + y_p)^2 b_2\Big] \\ &+ I_0^3\Big[\frac{1}{3}b_1^3 + \frac{1}{2}(2y_2 - 2y_p)b_1^2 + (y_2 - y_p)^2 b_1 + (x_3 - x_p)^2 b_1\Big] \\ &+ I_0^4\Big[\frac{1}{3}b_2^3 + \frac{1}{2}(-2x_3 + 2x_p)b_2^2 + (-x_3 + x_p)^2 b_2 + (y_4 - y_p)^2 b_2\Big] \end{aligned} \tag{44d}$$

$$\begin{aligned} m_q &= I_1^1(\frac{1}{2}b_1^2 - y_4 b_1 + y_p b_1) + I_1^2(x_1 b_2 + \frac{1}{2}b_2^2 - x_p b_2) \\ &+ I_1^3(y_2 b_1 + \frac{1}{2}b_1^2 - y_p b_1) + I_1^4(\frac{1}{2}b_2^2 - x_3 b_2 + x_p b_2) \end{aligned} \tag{44e}$$

$$m_s = -I_1^1 b_1 + I_1^3 b_1 \tag{44f}$$

$$
\begin{aligned}
m_{\omega} &= I_0^1(\frac{1}{2}A_1b_1^2+Cb_1)+I_0^2(\frac{1}{2}A_2b_2^2+A_1b_1b_2+Cb_2)+I_0^3(\frac{1}{2}A_3b_1^2+A_1b_1^2+A_2b_2b_1+Cb_1)\\
&+ I_0^4(\frac{1}{2}A_4b_2^2+A_1b_1b_2+A_2b_2^2+A_3b_1b_2+Cb_2) \qquad (44g)\\
m_2 &= I_2^1b_1+I_2^2b_2+I_2^3b_1+I_2^4b_2 \qquad (44h)\\
m_{2c} &= I_2^2b_2+I_2^4b_2 \qquad (44i)\\
m_{2q} &= I_2^1\Big[\frac{1}{3}(b_1-y_4+y_p)^3-\frac{1}{3}(-y_4+y_p)^3\Big]+I_2^2\Big[\frac{1}{3}(x_1+b_2-x_p)^3-\frac{1}{3}(x_1-x_p)^3\Big]\\
&+ I_2^3\Big[\frac{1}{3}(y_2+b_1-y_p)^3-\frac{1}{3}(y_2-y_p)^3\Big]+I_2^4\Big[\frac{1}{3}(b_2-x_3+x_p)^3-\frac{1}{3}(-x_3+x_p)^3\Big] \qquad (44j)\\
m_{2s} &= I_2^1b_1+I_2^3b_1 \qquad (44k)\\
m_{x2} &= I_0^1x_1^2b_1+I_0^2\Big[\frac{1}{3}(x_1+b_2)^3-\frac{1}{3}x_1^3\Big]+I_0^3x_3^2b_1+I_0^4\Big[-\frac{1}{3}(x_3-b_2)^3+\frac{1}{3}x_3^3\Big] \qquad (44l)\\
m_{y2} &= I_0^1\Big[-\frac{1}{3}(y_4-b_1)^3+\frac{1}{3}y_4^3\Big]+I_0^2y_2^2b_2+I_0^3\Big[\frac{1}{3}(y_2+b_1)^3-\frac{1}{3}y_2^3\Big]+I_0^4y_4^2b_2 \qquad (44m)\\
m_{\omega 2} &= I_0^1\Big[\frac{1}{3}(A_1b_1+C)^3/A_1-\frac{1}{3}C^3/A_1\Big]+I_0^2\Big[\frac{1}{3}(A_1b_1+A_2b_2+C)^3/A_2-\frac{1}{3}(A_1b_1+C)^3/A_2\Big]\\
&+ I_0^3\Big[\frac{1}{3}(C+A_1b_1+A_2b_2+A_3b_1)^3/A_3-\frac{1}{3}(A_1b_1+A_2b_2+C)^3/A_3\Big]\\
&+ I_0^4\Big[\frac{1}{3}(A_4b_2+A_1b_1+A_2b_2+A_3b_1+C)^3/A_4-\frac{1}{3}(C+A_1b_1+A_2b_2+A_3b_1)^3/A_4\Big] \qquad (44n)\\
m_{cs} &= 0 \qquad (44o)\\
m_{qc} &= I_2^2(x_1b_2+\frac{1}{2}b_2^2-x_pb_2)+I_2^4(-\frac{1}{2}b_2^2+x_3b_2-x_pb_2) \qquad (44p)\\
m_{qs} &= I_2^1(-\frac{1}{2}b_1^2+y_4b_1-y_pb_1)+I_2^3(y_2b_1+\frac{1}{2}b_1^2-y_pb_1) \qquad (44q)\\
m_{xs} &= -I_1^1x_1b_1+I_1^3x_3b_1 \qquad (44r)\\
m_{yc} &= I_1^2y_2b_2-I_1^4y_4b_2 \qquad (44s)\\
m_{q\omega} &= I_1^1\Big[\frac{1}{3}A_1b_1^3+\frac{1}{2}((-y_4+y_p)A_1+C)b_1^2+(-y_4+y_p)Cb_1\Big]\\
&+ I_1^2\Big[\frac{1}{3}A_2b_2^3+\frac{1}{2}((x_1-x_p)A_2+A_1b_1+C)b_2^2+(x_1-x_p)(A_1b_1+C)b_2\Big]\\
&+ I_1^3\Big[\frac{1}{3}A_3b_1^3+\frac{1}{2}((y_2-y_p)A_3+A_1b_1+A_2b_2+C)b_1^2+(y_2-y_p)(A_1b_1+A_2b_2+C)b_1\Big]\\
&+ I_1^4\Big[\frac{1}{3}A_4b_2^3+\frac{1}{2}((-x_3+x_p)A_4+C+A_1b_1+A_2b_2+A_3b_1)b_2^2\Big]\\
&+ I_1^4\Big[(-x_3+x_p)(C+A_1b_1+A_2b_2+A_3b_1)b_2\Big] \qquad (44t)\\
m_{x\omega} &= I_0^1(\frac{1}{2}x_1A_1b_1^2+x_1Cb_1)+I_0^2\Big[\frac{1}{3}A_2b_2^3+\frac{1}{2}(x_1A_2+A_1b_1+C)b_2^2+x_1(A_1b_1+C)b_2\Big]\\
&+ I_0^3\Big[\frac{1}{2}x_3A_3b_1^2+x_3(A_1b_1+A_2b_2+C)b_1\Big]\\
&+ I_0^4\Big[-\frac{1}{3}A_4b_2^3+\frac{1}{2}(x_3A_4-C-A_1b_1-A_2b_2-A_3b_1)b_2^2+x_3(C+A_1b_1+A_2b_2+A_3b_1)b_2\Big] \qquad (44u)\\
m_{y\omega} &= I_0^1\Big[-\frac{1}{3}A_1b_1^3+\frac{1}{2}(y_4A_1-C)b_1^2+y_4Cb_1\Big]+I_0^2\Big[\frac{1}{2}y_2A_2b_2^2+y_2(A_1b_1+C)b_2\Big]
\end{aligned}
$$

$$+ \; I_0^3\Big[\frac{1}{3}A_3b_1^3+\frac{1}{2}(y_2A_3+A_1b_1+A_2b_2+C)b_1^2+y_2(A_1b_1+A_2b_2+C)b_1\Big]$$
$$+ \; I_0^4\Big[\frac{1}{2}y_4A_4b_2^2+y_4(C+A_1b_1+A_2b_2+A_3b_1)b_2\Big] \tag{44v}$$

$$m_{\omega c} = I_1^2(\frac{1}{2}A_2b_2^2+A_1b_1b_2+Cb_2)+I_1^4(-\frac{1}{2}A_4b_2^2-A_1b_1b_2-A_2b_2^2-A_3b_1b_2-Cb_2) \tag{44w}$$

$$m_{\omega s} = I_1^1(-\frac{1}{2}A_1b_1^2-Cb_1)+I_1^3(\frac{1}{2}A_3b_1^2+A_1b_1^2+A_2b_2b_1+Cb_1) \tag{44x}$$

$$m_{xycs} = I_1^1(-y_4b_1+\frac{1}{2}b_1^2)+I_1^2(-x_1b_2-\frac{1}{2}b_2^2)+I_1^3(y_2b_1+\frac{1}{2}b_1^2)+I_1^4(x_3b_2-\frac{1}{2}b_2^2) \tag{44y}$$

$$m_{x\omega qs} = I_1^1\Big[\frac{1}{2}(-x_1-A_1)b_1^2+(y_4-y_p)x_1b_1-Cb_1\Big]$$
$$+ \; I_1^2\Big[-\frac{1}{3}b_2^3+\frac{1}{2}(-2x_1+x_p)b_2^2+(-x_1+x_p)x_1b_2\Big]$$
$$+ \; I_1^3\Big[\frac{1}{2}(A_3-x_3)b_1^2+(-y_2+y_p)x_3b_1+Cb_1+A_1b_1^2+A_2b_2b_1\Big]$$
$$+ \; I_1^4\Big[\frac{1}{3}b_2^3+\frac{1}{2}(-2x_3+x_p)b_2^2+(x_3-x_p)x_3b_2\Big] \tag{44z}$$

$$m_{y\omega qc} = I_1^1\Big[-\frac{1}{3}b_1^3+\frac{1}{2}(2y_4-y_p)b_1^2+(-y_4+y_p)y_4b_1\Big]$$
$$+ \; I_1^2\Big[\frac{1}{2}(y_2+A_2)b_2^2+(x_1-x_p)y_2b_2+A_1b_1b_2+Cb_2\Big]$$
$$+ \; I_1^3\Big[\frac{1}{3}b_1^3+\frac{1}{2}(2y_2-y_p)b_1^2+(y_2-y_p)y_2b_1\Big]$$
$$+ \; I_1^4\Big[\frac{1}{2}(y_4-A_4)b_2^2+(-x_3+x_p)y_4b_2-A_3b_1b_2-Cb_2-A_1b_1b_2-A_2b_2^2\Big] \tag{44aa}$$

where the warping constants A_1, A_2, A_3, A_4 and C can be found in Ref.[23]

References

[1] Vlasov VZ. Thin-walled elastic beams. 2nd Edition. Jerusalem, Israel: Israel Program for Scientific Translation; 1961.

[2] Gjelsvik A. The theory of thin-walled bars. New York: John Wiley and Sons Inc.; 1981.

[3] Timoshenko SP, Young DH and Weaver W. Vibration problems in engineering. 4^{th} Edition. New York: Wiley; 1974.

[4] Weaver W and Johnston PR. Structural dynamics by finite elements. Englewood Cliffs, NJ: Prentice-Hall; 1987.

[5] Kollar LP and Springer GS. Mechanics of composite structure. Cambridge University Press; 2003.

[6] Bank LC and Kao CH. The influence of geometric and material design variables on the free vibration of thin-walled composite material beams. J Vib Acoust Stress Reliab Des 1989;111:290-297.

[7] Bank LC and Kao CH. Dynamic Response of Thin-Walled Composite Material Timoshenko Beams. J Energ Resour 1990;112:149-154.

[8] Chandra R and Chopra I. Experimental-theoretical investigation of the vibration characteristics of rotating composite box beams. J Aircraft 1992;29(4):657-664.

[9] Song 0 and Librescu L. Free Vibration Of Anisotropic Composite Thin-Walled Beams Of Closed Cross-Section Contour. J Sound Vib 1993;167(1):129-147.

[10] Qin Z and Librescu L. On a shear-deformable theory of anisotropic thin-walled beams: further contribution and validations. Compos Struct 2002;56(4):345-358.

[11] Librescu L, Qin Z and Ambur DR. Implications of warping restraint on statics and dynamics of elastically tailored thin-walled composite beams. Int J Mech Sci 2003;45(8):1247-1267.

[12] Librescu L and Song 0. Thin-walled Composite Beams. Springer, 2006.

[13] Rand O. Free vibration of thin-walled composite blades. Compos Struct 1994;28(2):169-180.

[14] Armanios EA and Badir AM. Free vibration analysis of anisotropic thin-walled closed-section beams. AIAA J 1995;33(10):1905-10.

[15] Dancila DS and Armanios EA. The influence of coupling on the free vibration of anisotropic thin-walled closed-section beams. Int J Solids Struct 1998;35(23):3105-3119.

[16] Mitra M, Gopalakrishnan S and Bhat MS. A new super convergent thin walled composite beam element for analysis of box beam structures. Int J Solids Struct 2004;41(5-6):1491-1518.

[17] Cortinez VH and Piovan MT. Vibration and buckling of composite thin-walled beams with shear deformability. J Sound Vib 2002;258(4-5):701-723.

[18] Piovan MT and Cortinez VH. Mechanics of shear deformable thin-walled beams made of composite materials. Thin-Walled Struct 2007;45(1):37-62

[19] Machado SP, Filipich CP and Cortinez VH. Parametric vibration of thin-walled composite beams with shear deformation. J Sound Vib 2007;305(4-5):563-581.

[20] Shadmehri F, Haddadpour H and Kouchakzadeh MA. Flexural-torsional behavior of thin-walled composite beams with closed cross-section. Thin-Walled Struct 2007;45(7-8):699-705.

[21] Vo TP and Lee J. Free vibration of thin-walled composite box beams. Compos Struct 2007;84(1):11-20.

[22] Vo TP and Lee J. Flexural-torsional behavior of thin-walled composite box beams using shear-deformable beam theory. Eng Struct 2008;30(7):1958-1968.

[23] Vo TP and Lee J. Flexural-torsional behavior of thin-walled closed-section composite box beams. Eng Struct 2007;29(8):1774-1782.

[24] Jones RM. Mechanics of composite materials. New York: Hemisphere Publishing Corp.; 1975.

[25] Lee J. Flexural analysis of thin-walled composite beams using shear-deformable beam theory. Compos Struct 2005;70(2):212-222.

CAPTIONS OF FIGURES

Figure 1: Definition of coordinates and generalized displacements in thin-walled closed sections.

Figure 2: Stacking sequences of thin-walled composite box beam.

Figure 3: Effects of shear deformation on the first three natural frequencies with respect to fiber angle change in the flanges and webs for a clamped composite beam with ratio $l/b_1 = 20$.

Figure 4: Mode shapes of the flexural-torsional-shearing components for the first mode $\omega_1 = 25.941$ of a clamped composite beam with the fiber angle 15° in the flanges and webs with $l/b_1 = 20$.

Figure 5: Mode shapes of the flexural-torsional-shearing components for the second mode $\omega_2 = 33.903$ of a clamped composite beam with the fiber angle 15° in the flanges and webs with $l/b_1 = 20$.

Figure 6: Mode shapes of the flexural-torsional-shearing components for the third mode $\omega_3 = 65.581$ of a clamped composite beam with the fiber angle 15° in the flanges and webs with ratio $l/b_1 = 20$.

Figure 7: Effects of shear deformation on the first three natural frequencies with respect to fiber angle change in the left web and bottom flange for a clamped composite beam with ratio $l/b_1 = 50$.

Figure 8: Effects of shear deformation on the first three natural frequencies with respect to fiber angle change in the right web and bottom flange for a clamped composite beam with ratio $l/b_1 = 20$.

Figure 9: Mode shapes of the flexural-torsional-shearing components for the first mode $\omega_1 = 15.730$ of a clamped composite beam with the fiber angle 30° in the right web and bottom flange with ratio $l/b_1 = 20$.

Figure 10: Mode shapes of the flexural-torsional-shearing components for the second mode $\omega_2 = 23.330$ of a clamped composite beam with the fiber angle 30° in the right web and bottom flange with ratio $l/b_1 = 20$.

Figure 11: Mode shapes of the flexural-torsional-shearing components for the third mode $\omega_3 = 41.511$ of a clamped composite beam with the fiber angle 30° in the right web and bottom flange with ratio $l/b_1 = 20$.

Figure 12: Variation of the natural frequencies $\omega_{x_1}, \omega_{y_1}, \omega_{\theta_1}$ of a simply supported composite beam ($l/b_1 = 10$) with respect to modulus ratio change.

Figure 13: Effect of the warping restraint on the natural frequencies $\omega_{x_1}, \omega_{y_1}, \omega_{\theta_1}$ of a cantilever composite beam ($l/b_1 = 10$) with respect to modulus ratio change.

Figure 14: Geometry of thin-walled composite box section.

CAPTIONS OF TABLES

Table I: Material properties and geometric characteristics of a cantilever composite box beam for verification.

Table II: Comparison of theoretical and experimental natural frequencies (Hz) of a cantilever composite box beam with CAS and CUS lay-ups.

Table III: Natural frequencies (Hz) of a cantilever composite box beam with $[0/90]_A$ lay-up.

Table IV: Nondimensional natural frequencies respect to the fiber angle change in the flanges and webs with ratio $l/b_1 = 20$.

Table V: Nondimensional natural frequencies respect to the fiber angle change in the left web and bottom flange with ratio $l/b_1 = 20$.

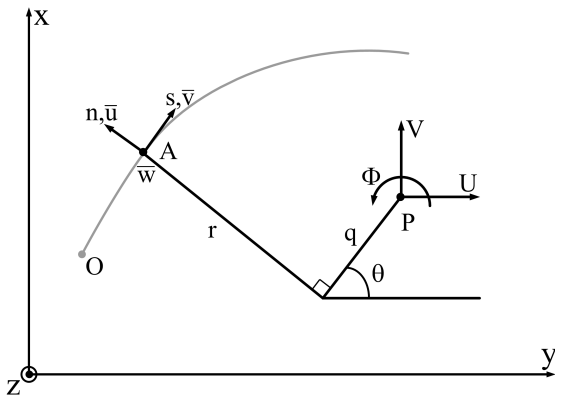

FIG. 1 Definition of coordinates and generalized displacements in thin-walled closed sections.

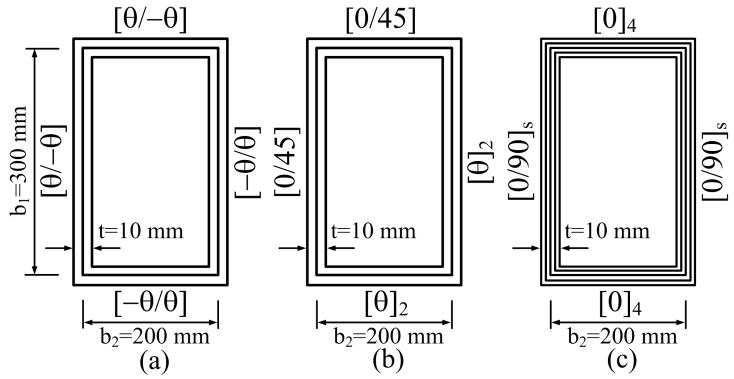

FIG. 2 Stacking sequences of thin-walled composite box beam.

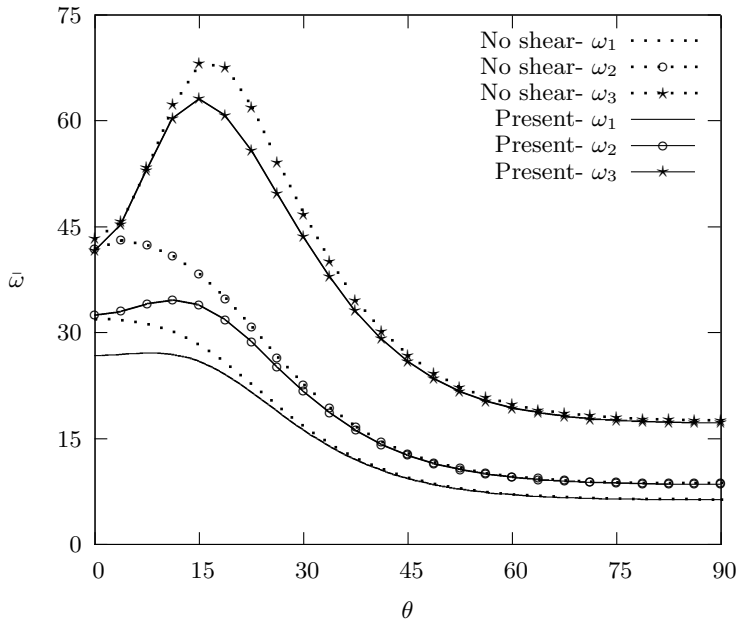

FIG. 3 Effects of shear deformation on the first three natural frequencies with respect to fiber angle change in the flanges and webs for a clamped composite beam with ratio $l/b_1 = 20$.

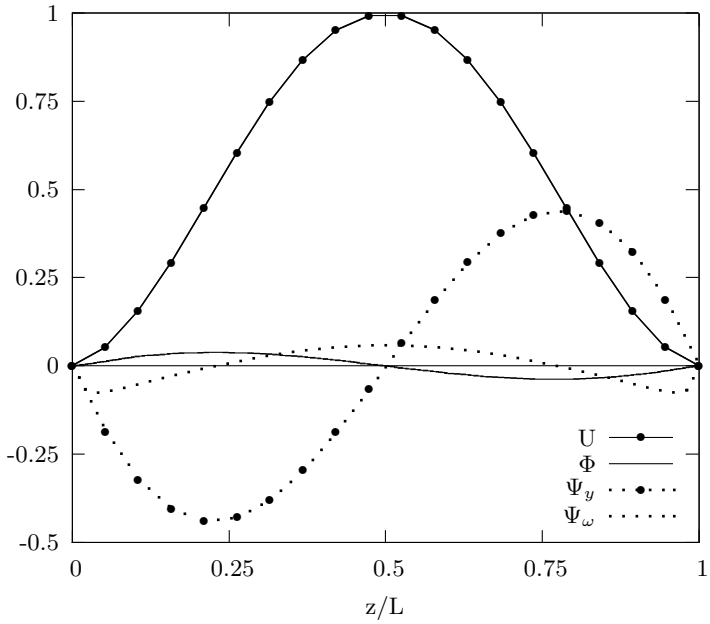

FIG. 4 Mode shapes of the flexural-torsional-shearing components for the first mode $\omega_1 = 25.941$ of a clamped composite beam with the fiber angle 15° in the flanges and webs with ratio $l/b_1 = 20$.

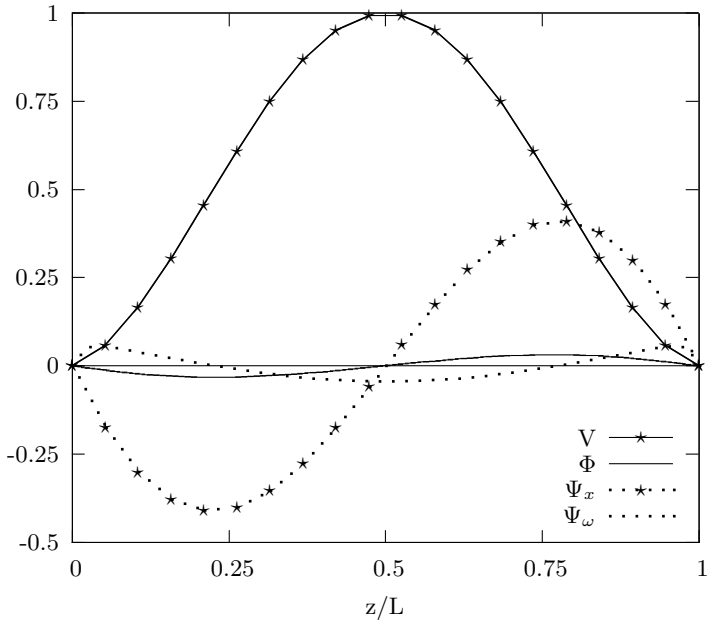

FIG. 5 Mode shapes of the flexural-torsional-shearing components for the second mode $\omega_2 = 33.903$ of a clamped composite beam with the fiber angle 15° in the flanges and webs with ratio $l/b_1 = 20$.

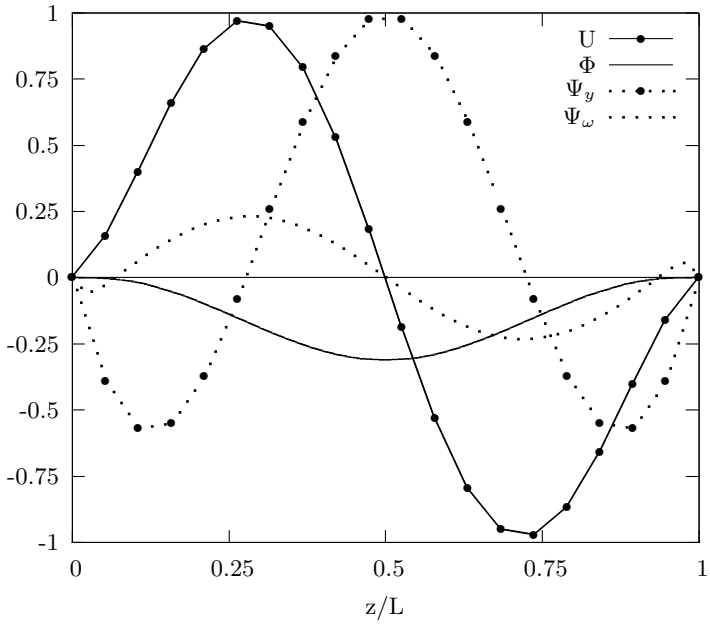

FIG. 6 Mode shapes of the flexural-torsional-shearing components for the third mode $\omega_3 = 65.581$ of a clamped composite beam with the fiber angle 15° in the flanges and webs with ratio $l/b_1 = 20$.

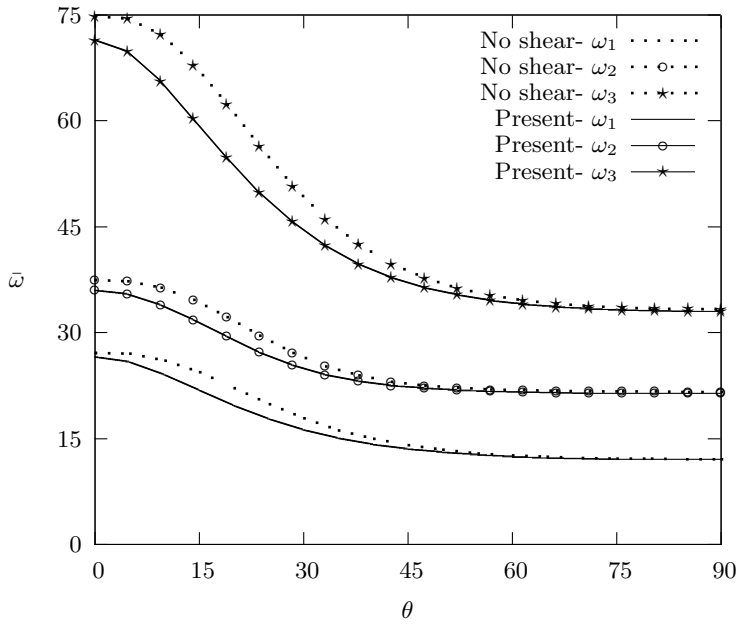

FIG. 7 Effects of shear deformation on the first three natural frequencies with respect to fiber angle change in the right web and bottom flange for a clamped composite beam with ratio $l/b_1 = 50$.

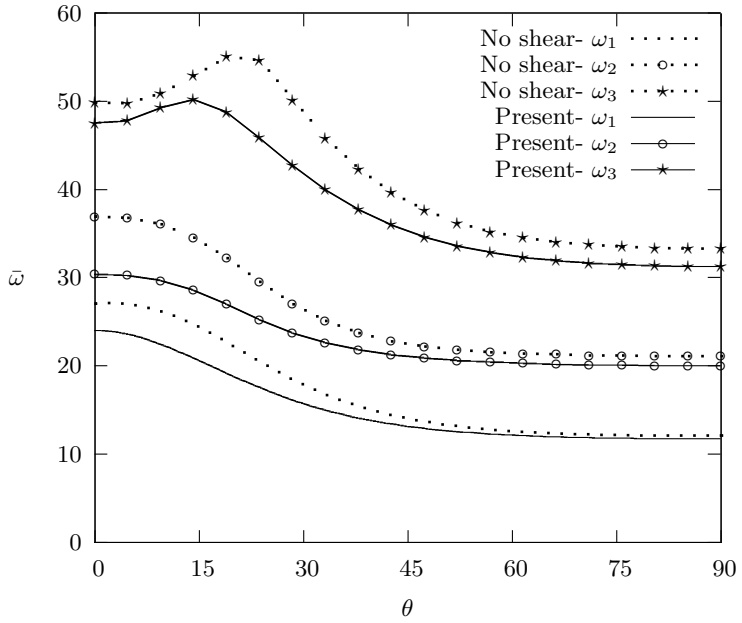

FIG. 8 Effects of shear deformation on the first three natural frequencies with respect to fiber angle change in the right web and bottom flange for a clamped composite beam with ratio $l/b_1 = 20$.

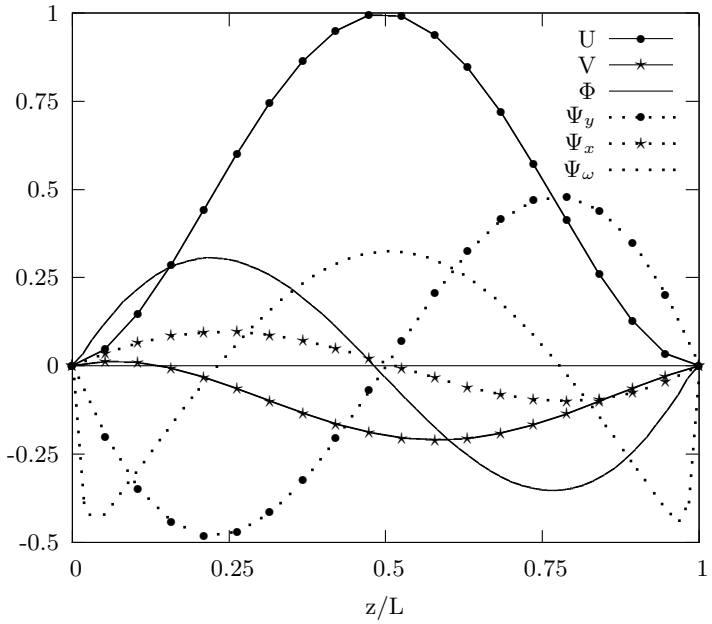

FIG. 9 Mode shapes of the flexural-torsional-shearing components for the first mode $\omega_1 = 15.730$ of a clamped composite beam with the fiber angle 30° in the right web and bottom flange with ratio $l/b_1 = 20$.

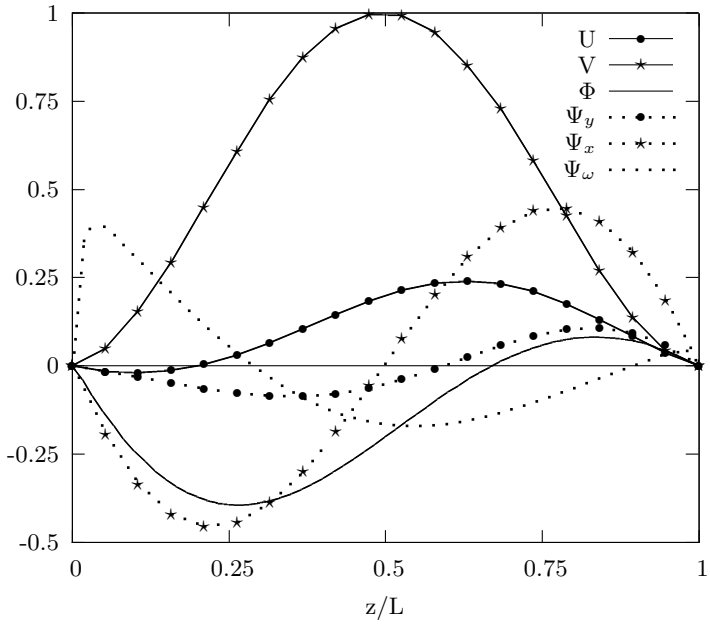

FIG. 10 Mode shapes of the flexural-torsional-shearing components for the second mode $\omega_2 = 23.330$ of a clamped composite beam with the fiber angle 30° in the right web and bottom flange with ratio $l/b_1 = 20$.

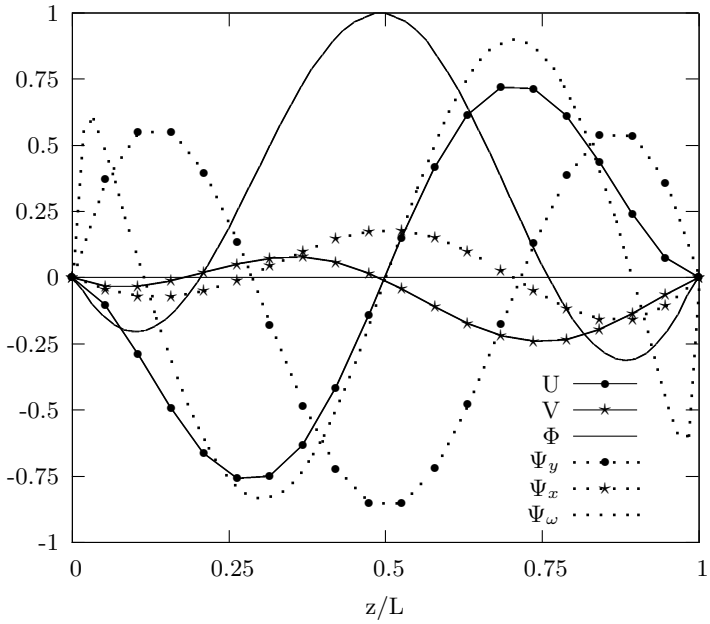

FIG. 11 Mode shapes of the flexural-torsional-shearing components for the third mode $\omega_3 = 41.511$ of a clamped composite beam with the fiber angle 30° in the left web and bottom flange with ratio $l/b_1 = 20$.

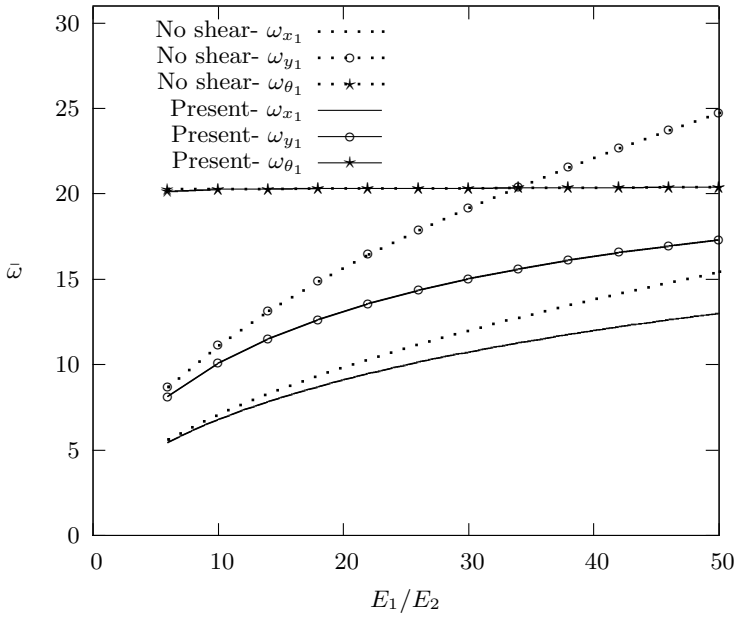

FIG. 12 Variation of the natural frequencies $\omega_{x_1}, \omega_{y_1}, \omega_{\theta_1}$ of a simply supported composite beam ($l/b_1 = 10$) with respect to modulus ratio change.

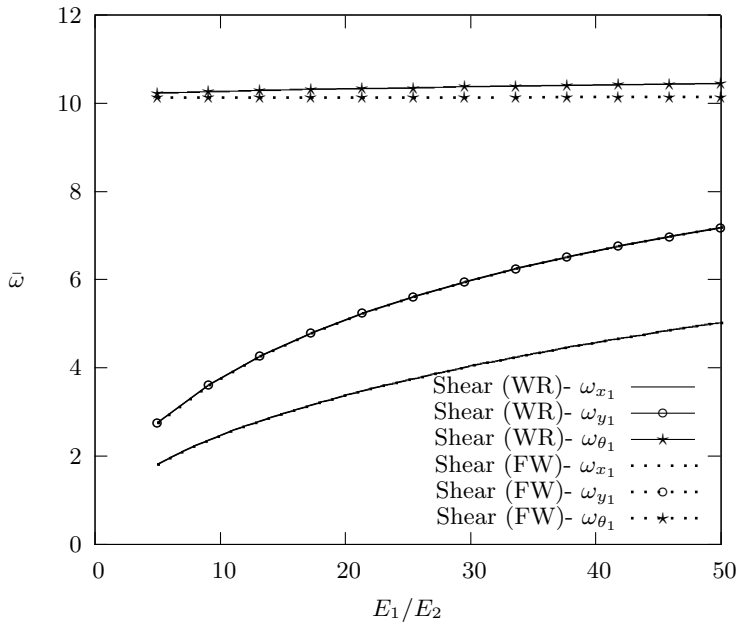

FIG. 13 Effect of the warping restraint on the natural frequencies $\omega_{x_1}, \omega_{y_1}, \omega_{\theta_1}$ of a cantilever composite beam ($l/b_1 = 10$) with respect to modulus ratio change.

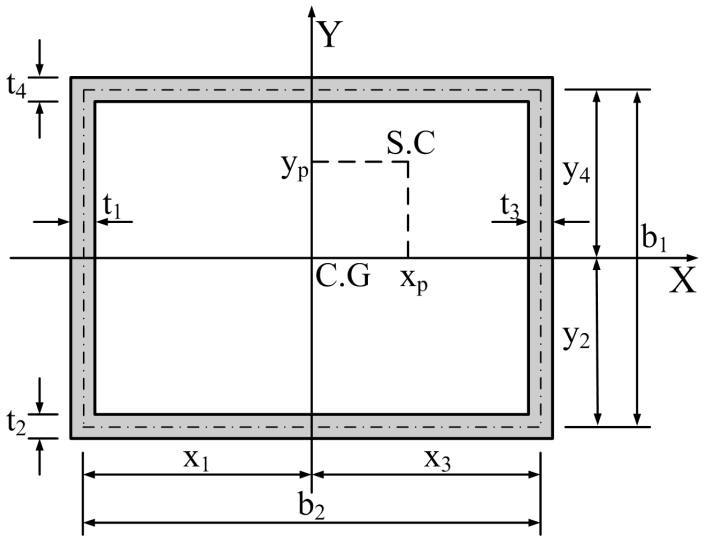

FIG. 14 Geometry of thin-walled composite box section.

TABLE I Material properties and geometric characteristics of a cantilever composite box beam for verification.

Parameters	Value
Material properties	
E_1, psi (GPa)	$20.59 \times 10^6 (141.9)$
E_2, psi (GPa)	$1.42 \times 10^6 (9.78)$
$G_{12} = G_{13}$, psi (GPa)	$0.89 \times 10^6 (6.13)$
G_{23}, psi (GPa)	$0.696 \times 10^6 (4.80)$
ν_{12}	0.42
$\rho, \mathrm{lbs}^2/\mathrm{in}^4 (\mathrm{kg}/\mathrm{m}^3)$	$0.1352 \times 10^{-3} (1445)$
Geometry properties	
Length, in.(mm)	33.25 (844.5)
Outer width, in.(mm)	0.953 (24.21)
Outer depth, in.(mm)	0.537 (13.46)
Wall thickness, in.(mm)	0.03 (0.762)
Ply thickness, in.(mm)	0.005 (0.127)
Number of layers	6

TABLE II Comparison of theoretical and experimental natural frequencies (Hz) of a cantilever composite box beam with CAS and CUS lay-ups.

Lay-up	Flanges		Webs		Mode	Ref.[8]	Ref.[10]	Ref.[21]	Present
	Top	Bottom	Left	Right					
CAS2	$[30]_6$	$[-30]_6$	$[30/-30]_3$	$[30/-30]_3$	1TV	20.96	21.80	22.07	21.80
CAS3	$[45]_6$	$[-45]_6$	$[45/-45]_3$	$[45/-45]_3$	1TV	16.67	15.04	15.13	14.86
CUS1	$[15]_6$	$[15]_6$	$[15]_6$	$[15]_6$	1VB	28.66	30.06	38.65	32.02
CUS2	$[0/30]_3$	$[0/30]_3$	$[0/30]_3$	$[0/30]_3$	1VB	30.66	34.58	35.53	34.47
CUS3	$[0/45]_3$	$[0/45]_3$	$[0/45]_3$	$[0/45]_3$	1VB	30.00	32.64	32.52	32.41

TABLE III Natural frequencies (Hz) of a cantilever composite box beam with $[0/90]_A$ lay-up.

Mode	Ref.[16]			Ref.[21]	Present
	No shear	With shear	ANSYS		
1	31.06	31.02	30.99	31.30	31.04
2	49.34	49.17	49.19	49.86	49.54
3	194.57	192.55	187.22	196.16	194.06
4	308.75	301.63	298.13	312.48	304.79
7	862.40	817.54	794.24	874.97	826.46
11	1757.35	1642.38	1680.80	1779.29	1659.92
12	2107.33	2107.28	2111.70	2145.28	2145.09
14	2619.31	2381.89	2349.40	2657.98	2437.71
15	2771.02	2409.78	2418.00	2834.36	2440.04
16	3321.34	3220.05	3198.00	3419.13	3262.88

TABLE IV Nondimensional natural frequencies respect to the fiber angle change in the flanges and webs with ratio $l/b_1 = 20$.

Fiber	Orthotropy solution				FEM		
angle	w_{x_1}	w_{y_1}	w_{θ_1}	w_{x_2}	w_1	w_2	w_3
0	26.759	32.442	41.594	63.252	26.759	32.442	41.594
15	25.959	33.911	71.530	65.630	25.941	33.903	65.581
30	16.215	21.716	57.085	43.242	16.202	21.709	43.209
45	9.354	12.593	33.801	25.358	9.350	12.591	25.348
60	7.041	9.486	25.574	19.163	7.041	9.486	19.161
75	6.439	8.669	23.367	17.531	6.439	8.669	17.530
90	6.327	8.516	22.944	17.226	6.327	8.516	17.226

TABLE V Nondimensional natural frequencies respect to the fiber angle change in the left web and bottom flange with ratio $l/b_1 = 20$.

Fiber	Orthotropy solution				FEM		
angle	w_{x_1}	w_{y_1}	w_{θ_1}	w_{x_2}	w_1	w_2	w_3
0	24.151	30.711	48.031	59.286	24.027	30.390	47.507
15	23.584	30.882	63.220	59.742	20.595	28.316	51.170
30	18.760	25.229	64.379	49.079	15.730	23.330	41.511
45	14.798	21.075	54.203	39.166	13.163	21.049	35.045
60	13.511	19.798	50.769	35.820	12.157	20.346	32.405
75	13.192	19.448	48.327	34.952	11.814	20.082	31.474
90	13.132	19.372	47.393	34.780	11.737	20.007	31.255